Application Note

Zurich Instruments

Femtosecond noise correlation spectroscopy

Applications: Optics, noise, correlations

Products: UHFLI

Release date: February 2025

Introduction

Fluctuations are a driving force of a rich variety of fundamental physical phenomena. For example, thermal fluctuations of spins critically determine the magnetic properties of correlated spin systems [1]. Therefore, the study of spin fluctuations is of paramount importance for the emerging field of spintronics, in which contemporary electronics is pursued to be complemented by the inherent spin degree of freedom [2]. Due to their ultrafast magnon frequencies, antiferromagnets (AFM) are promising candidates to accelerate spintronic applications to the terahertz regime [3]. For this reason, Femtosecond noise correlation spectroscopy (FemNoC) was recently established as a tool to probe the ultrafast fluctuation dynamics of thermally populated magnons. It successfully revealed picosecond stochastic switching in the spin reorientation transition regime of the antiferromagnet $Sm_{0.7}Er_{0.3}FeO_3$ [4]. Such dynamics were so far not measurable using conventional, deterministic ultrafast spectroscopy techniques (e.g. pump-probe).

FemNoC utilises two differently colored and linearly polarised femtosecond pulse trains to probe the magnetisation fluctuations, which spontaneously arise in a magnetic sample. In a first step, the pulse trains are transmitted through the sample with a variable time delay Δt. Here, transient out-of-plane magnetisation fluctuations δM_z imprint as polarisation noise $\delta\alpha$ onto the pulses via the Faraday effect. Using a dichroic mirror, the probe beams are then separated into two separate detection branches, where their respective polarisation state is recorded. These detectors yield an output signal with a periodicity of the repetition rate f_{rep} of the laser pulse train. To extract the fluctuation component of the detector outputs, subharmonic demodulation is performed for each branch in a UHFLI 600 MHz Lock-in Amplifier. This step removes any static background and spurious 1/f like noise components arising in the detection electronics. Lastly, the subharmonic outputs are multiplied in real time and consecutively averaged to obtain the correlated polarisation fluctuations. During this process, uncorrelated background noise, e.g. Johnson noise in the electronics and shot noise of the optical probes, is eliminated. By variation of the pulse-to-pulse time delay Δt, the full polarisation noise correlation function $\langle \Delta\delta\alpha_1(t) \cdot \Delta\delta\alpha_2(t+\Delta t)\rangle$ is revealed.

Methods

Figure 1 shows a schematic illustration of the experimental setup. Two spectrally detuned probing pulse trains are prepared from a single femtosecond Er:fibre laser with 1550 nm wavelength and 40 MHz repetition rate. A dichroic mirror (DM) spectrally and spatially separates the input beam into two branches with 767 nm and 775 nm wavelength, respectively. The reflected beam (light blue) passes a delay line, where a time delay Δt is introduced with respect to the transmitted beam (dark blue). Next, the two beams are recombined in a second DM. Subsequently, a polariser sets the mean polarisation to $\langle\alpha\rangle = 45°$. Afterwards, they are focussed onto the magnetic sample. Here, additional polarisation noise $\delta\alpha_1(t) \propto \delta M_z(t)$ and $\delta\alpha_2(t+\Delta t) \propto \delta M_z(t+\Delta t)$ is imprinted onto the femtosecond probes via the Faraday effect by parallel spontaneous magnetisation fluctuations δM_z in the sample. Using another DM, the beams are guided into two separate detection branches, each consisting of a half wave plate (HWP), a Wollaston prism (WP)

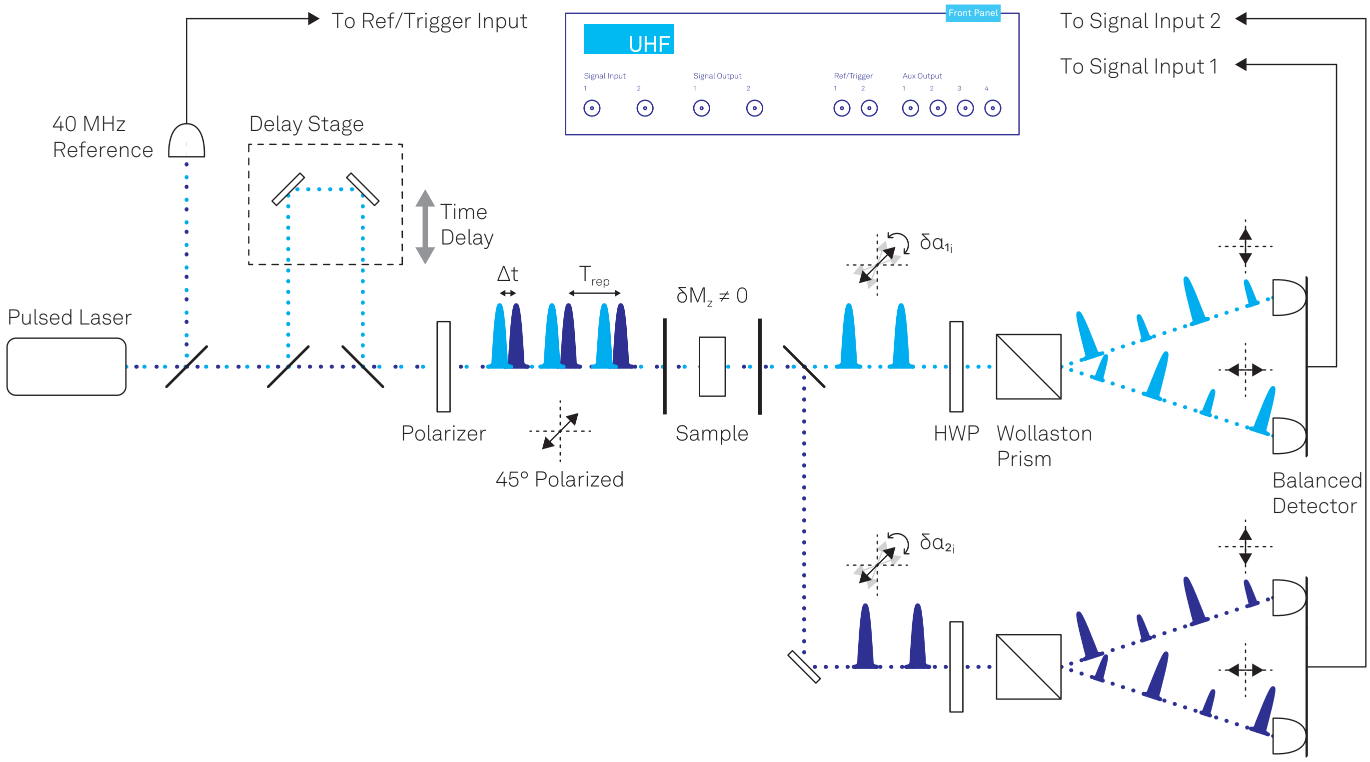

Figure 1. Schematic illustration of the experimental setup. Two independent femtosecond laser pulse trains with marginally different wavelength are used to probe spontaneous magnetisation fluctuations in a magnetic sample.

and a pair of balanced photodetectors (BPD). The WPs split the incoming probe beams into their respective s- and p-polarisation components, which are subsequently focussed onto the BPDs. As a result, the BPDs yield an output voltage $V_{1,2}(t)$ proportional to the difference in optical power $P_s - P_p$ of s- and p-polarized components. This power difference is directly proportional to the polarisation fluctuation $\delta\alpha_{1,2}(t)$ in case the mean polarisation is $\langle\alpha_{1,2}\rangle = 45°$ (balanced) [5]:

$$V_{1,2}(t) \propto P_s - P_p = 2P_0\delta\alpha_{1,2}(t) \qquad (1)$$

Here, P_0 is the average power of a single probe beam. Although the mean input polarisation is chosen to be $\langle\alpha_{1,2}\rangle = 45°$, static polarisation rotations may emerge due to unwanted sample effects, such as birefringence and static magnetisation components. The HWPs are used to compensate for this static polarisation component and rebalance the beams polarisation to $\langle\alpha_{1,2}\rangle = 45°$.

The detector outputs serve as the signal inputs 1 and 2 of the UHFLI, respectively. They are dominated by the repetition rate $f_{rep} = 2\pi/\omega_{rep}$ of the pulsed laser, which in our case is 40 MHz. Instead, we are interested in the fluctuation component, which is maximal at the subharmonic frequency $f_{rep}/2 = 20\text{MHz}$ (pulse-to-pulse fluctuations) [6]. To fully take advantage of the UHFLI's digitisation depth, we interpose an amplifier and a 20 MHz bandpass filter between detector output and lock-in. This suppresses spurious low-frequency signals and the dominant 40 MHz component, while amplifying the 20 MHz pulse-to-pulse fluctuations of interest.

Inside the UHFLI, subharmonic demodulation of the inputs is carried out: First, $V_{1,2}(t)$ are multiplied (mixed) with a complex reference sinusoidal $V_r(t) = Ae^{i((\omega_{rep}/2)t+\theta)}$ with amplitude A, phase θ and subharmonic angular frequency $\omega_{rep}/2$. We obtain the $\omega_{rep}/2$ reference frequency by guiding part of the pulsed beam onto a photodiode, which consequently outputs a 40 MHz voltage. This 40 MHz voltage is connected to the Ref/Trigger of the UHFLI and the frequency is tracked with a phase-locked loop (PLL). An internal oscillator at 20 MHz can be directly obtained by configuring the PLL on the second subharmonic. The mixing is followed by low-pass filtering with a time constant TC. This process is known as dual-phase demodulation [7]. In order to obtain a simplified mathematical expression, we here approximate the low-pass filter function with a moving average and describe the demodulation result by

$$\begin{aligned} Z_{1,2} &\approx \frac{1}{TC_{1,2}}\int_0^{TC_{1,2}} V_{1,2}(t)V_r(t)dt \\ &= \frac{Ae^{i\theta}}{TC_{1,2}}\int_0^{TC_{1,2}} V_{1,2}(t)e^{i(\omega_{rep}/2)t}dt \end{aligned} \qquad (2)$$

where $Z_{1,2} = X_{1,2} + iY_{1,2}$ is the complex output of the demodulation channel 1 and 2 with time constant $TC_{1,2}$. It can be shown that subharmonic demodulation directly yields

$$Z_{1,2} \approx Ae^{i\theta}\langle\Delta\delta V_{1,2}(t)\rangle_{TC_{1,2}}. \qquad (3)$$

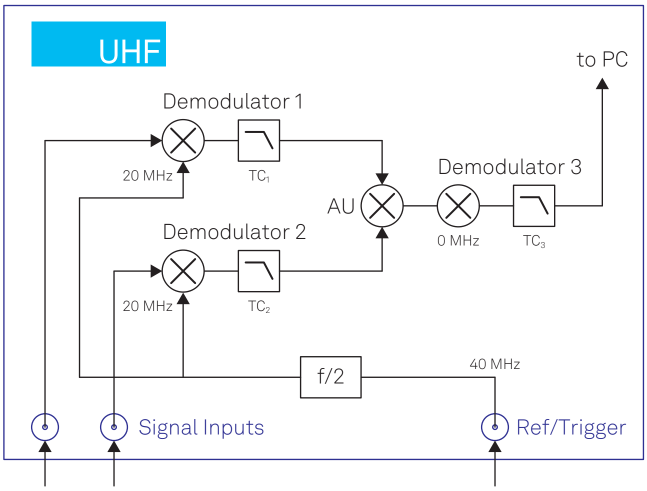

Figure 2. Schematic illustration of the data processing in the UHFLI. The outputs of the balanced photodetectors are provided to the two signal input channels of the UHFLI, and demodulated at 20 MHz in Demodulator 1 and Demodulator 2, resulting in the pulse-to-pulse fluctuations. Next, the demodulator outputs are multiplied in real time in the arithmetic unit (AU) and subsequently averaged in Demodulator 3. This process yields the correlation of the input signals.

This can be interpreted as the averaged pulse-to-pulse fluctuation $\langle \Delta\delta V_{1,2}(t)\rangle_{TC_{1,2}}$ around the subharmonic frequency multiplied by a phase factor $e^{i\theta}$ [5]. Next, the real parts

$$\begin{aligned} \mathrm{Re}(Z_{1,2}(t)) &= X_{1,2}(t) \\ &= \cos(\theta_{1,2})\langle \Delta\delta V_{1,2}(t)\rangle_{TC_{1,2}} \end{aligned} \quad (4)$$

of the demodulation channels 1 and 2 are sent to the arithmetic unit (AU) of the UHFLI, where real-time multiplication of $\Delta\delta V_1(t)$ and $\Delta\delta V_2(t+\Delta t)$ is performed. To obtain the correlated noise, the product $\cos(\theta_1)\cos(\theta_2)\langle\Delta V_1(t)\rangle_{TC_1}\rangle\langle\Delta V_2(t+\Delta t)\rangle_{TC_2}$ is averaged by demodulation with a DC reference with time constant TC_3. This process reveals the correlation output

$$\begin{aligned} V_{corr}(\Delta t) \propto\ & \cos(\theta_1)\cos(\theta_2) \\ & \cdot\langle\langle\Delta\delta V_1(t)\rangle_{TC_1}\langle\Delta\delta V_2(t+\Delta t)\rangle_{TC_2}\rangle_{TC_3}. \end{aligned} \quad (5)$$

Note that the output of the arithmetic unit is internally scaled with a factor of 1/V resulting in the output $V_{corr}(\Delta t)$ being in the unit of V instead of V^2. The outputs of the subharmonic demodulation channels are directly proportional to the magnetic noise at the transmission time of the femtosecond probes $\Delta\delta V_1(t) \propto \delta\alpha_1(t) \propto \delta M_z(t)$ and $\Delta\delta V_2(t+\Delta t) \propto \delta\alpha_2(t+\Delta t) \propto \delta M_z(t+\Delta t)$. Consequently, by varying the relative time delay Δt of the probe beams, the ultrafast magnetisation autocorrelation is directly retrieved

$$\begin{aligned} V_{corr}(\Delta t) \propto\ & \cos(\theta_1)\cos(\theta_2) \\ & \cdot\langle\langle\delta M_z(t)\rangle_{TC_1}\langle\delta M_z(t+\Delta t)\rangle_{TC_2}\rangle_{TC_3}. \end{aligned} \quad (6)$$

From equation 6 it becomes clear that a multitude of lock-in settings can be tuned to optimise the signal-to-noise ratio of $V_{corr}(\Delta t)$:

1. The relative phases θ_1 and θ_2 between the signal inputs 1 and 2 and the subharmonic reference need to be adjusted. Setting both to either 0° or 180° maximizes the correlation output, while setting one of the phases to either 90° or 270° results in the correlation output being zero.
2. The time constants $TC_{1,2}$ need to be long enough to capture the difference between two consecutive pulses, but should be as low as possible to avoid averaging out of the stochastic spin fluctuations. The ideal setting is $TC_{1,2} \approx 2T_{rep}$.
3. TC_3 should be chosen as long as possible to allow for sufficient averaging of the correlation signal and suppression of background noise. However, this comes with the trade off of an increased measurement time.

Results

Using FemNoC, Weiss et al. measured the magnetic correlation function of the antiferromagnet $Sm_{0.7}Er_{0.3}FeO_3$. In their work, the sample was held at constant temperature $T = 294.2$K and out-of-plane magnetic field $B = 28 \pm 5$mT. The measurements were performed in a time window from $\Delta t = -85$ps to $\Delta t = +85$ps in 2 ps steps [5]. This was repeated for different lock-in settings to investigate their influence on the signal-to-noise ratio of the correlation signal. Figure 3a shows the time-domain correlation function measured for different time constants $TC = TC_1 = TC_2$ of the subharmonic demodulation. The measured waveforms are symmetric around zero, which is characteristic for an autocorrelation. Furthermore, they show an oscillation around the zero-crossing line, lasting for several tens of picoseconds. The oscillation with wavelength of ≈20 ps (frequency f≈50 GHz) is identified as the quasiferromagnetic magnon mode [4, 5]. Evidently, the (time-zero) amplitude of the correlation function decreases with an increase in TC in accordance with our prediction that preaveraging of the pulse-to-pulse fluctuation occurs. The amplitude scales as $1/TC^2$ due to the correlation being quadratic with the pulse-to-pulse fluctuation amplitude (see Equation 5)[5]. Figure 3b depicts the correlation waveforms recorded for different TC_3. Here, the amplitude remains constant as a function of TC_3, while the background noise drastically increases upon lowering TC_3. This can be understood by the fact that background noise is only efficiently suppressed when the correlation product is sufficiently averaged. At last, Weiss et al. investigated the time-zero correlation amplitude as a function of the reference phases $\theta_{1,2}$ of the demodulation channels 1 and 2. The results in Figure 3c clearly show the $\cos(\theta_1)\cos(\theta_2)$ dependence predicted in Equation 5, highlighting the importance of adjusting the phases to maximize the correlation signal.

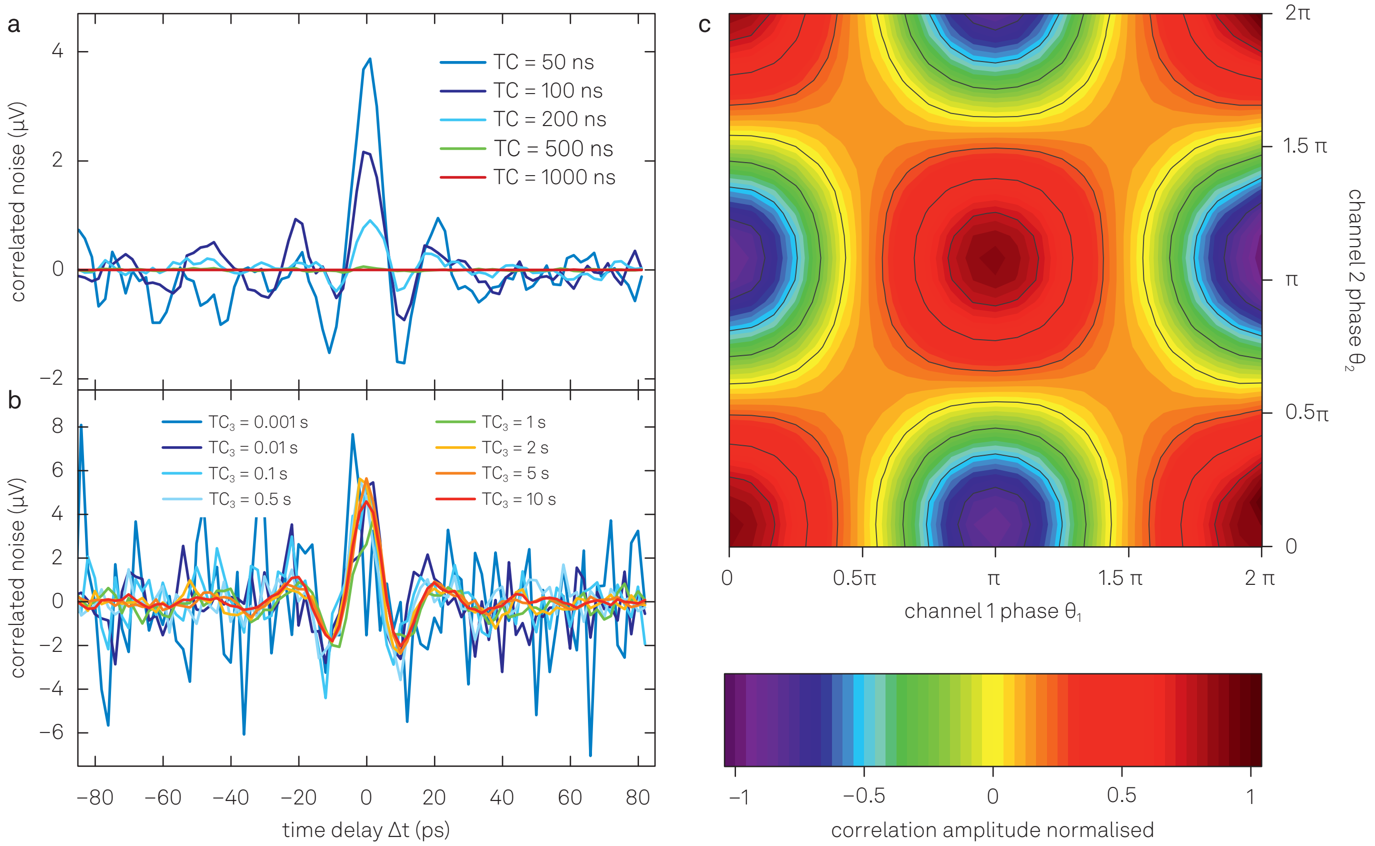

Figure 3. Dependence of the correlation waveforms measured in $Sm_{0.7}Er_{0.3}FeO_3$ on different lock-in settings. a) Correlation waveforms recorded for different time constants $TC = TC_1 = TC_2$ of the subharmonic demodulation. b) Correlation waveforms recorded for different time constants TC_3 of Demodulator 3. c) Dependence of the $\Delta t = 0$ correlation amplitude on the phases θ_1 and θ_2 of the reference sinusoidals in demodulator 1 and demodulator 2. Figure adapted from Ref. [5]

Conclusion

Femtosecond noise correlation spectroscopy (FemNoC) was recently introduced by Weiss et al. to probe the ultrafast fluctuation dynamics of thermally populated magnons [4]. In this application note, we give a guide how to implement FemNoC using the UHFLI and discuss how to choose optimal lock-in settings to obtain a clear signal.

Acknowledgments

We would like to thank M. A. Weiss (marvin.weiss@uni-konstanz.de), A. Leitenstorfer, S. T. B. Goennenwein (Department of Physics, University of Konstanz, D-78457 Konstanz, Germany) and Takayuki Kurihara (The Institute of Solid State Physics, The University of Tokyo) for providing the data and their contribution in authoring this application note.

References

[1] H. Falk and L.W. Bruch. Susceptibility and fluctuation. Phys. Rev., 180:442, 1969.

[2] S.D. Bader and S.S.P. Parkin. Spintronics. Annu. Rev. Condens. Matter Phys., 1:71, 2010.

[3] F. Bloch. Nuclear induction. Phys. Rev., 70:460, 1949.

[4] M.A. Weiss, F.S. Herbst, J. Schlegel, T. Dannegger, M. Evers, A. Donges, M. Nakajima, A. Leitenstorfer, S.T.B. Goennenwein, U. Nowak, and T. Kurihara. Discovery of ultrafast spontaneous spin switching in an antiferromagnet by femtosecond noise correlation spectroscopy. Nat. Commun., 14:7651, 2023.

[5] M. A. Weiss, F. S. Herbst, S. Eggert, M. Nakajima, A. Leitenstorfer, S. T. B. Goennenwein, and T. Kurihara. Subharmonic lock-in detection and its optimization for femtosecond noise correlation spectroscopy. Review of Scientific Instruments, 95:083005, 2024.

[6] Y. Ozeki, Y. Kitagawa, K. Sumimura, N. Nishizawa, W. Umemura, S. Kajiyama, K. Fukui, and K. Itoh. Stimulated raman scattering microscope with shot noise limited sensitivity using subharmonically synchronized laser pulses. Opt. Express, 18:13708, 2010.

[7] Zurich Instruments. Principles of lock-in detection, whitepaper. Whitepaper.